CrystEngComm

ROYAL SOCIETY OF CHEMISTRY

PAPER

View Article Online
View Journal | View Issue

Cite this: *CrystEngComm*, 2020, **22**, 448

An investigation of the polymorphism of a potent nonsteroidal anti-inflammatory drug flunixin†

Hao Liu,[a] Xing Yang,[a] Shanyu Wu,[b] Mingtao Zhang,[b] Sean Parkin,[c] Shuang Cao,[a] Tonglei Li,[d] Faquan Yu‡[a] and Sihui Long *[a]

Received 14th October 2019,
Accepted 22nd November 2019

DOI: 10.1039/c9ce01619h

rsc.li/crystengcomm

Flunixin [2-(3-trifluoromethyl-2-methyl-phenylamino)-nicotinic acid, FLX], a potent nonsteroidal anti-inflammatory drug widely used in veterinary medicine, was found to exist in at least two crystal forms (I and II), in contrast to clonixin [2-(3-chloro-2-methyl-phenylamino)-nicotinic acid, CLX], which exists in four solvent-free forms and multiple solvates. Form I was harvested from a variety of solvents and characterized by single-crystal X-ray diffraction, PXRD, FT-IR, and Raman spectroscopy. Its crystal structure is sustained on the strong acid–pyridine hydrogen bond. Form II was generated by thermal treatment of form I. Other aspects of this polymorphic system were investigated both experimentally and theoretically. Quantum chemistry calculations were performed to shed light on the lack of polymorphism from solution-phase crystallization. Conformational scan of the dihedral angle C2–N7–C8–C9 (τ) revealed two stable conformations, one with τ near 170°, and the other near 70°, corresponding to the molecule in the crystal. Hirshfeld analysis accounted for the major intermolecular interactions contributing to the overall stability of the crystal.

1. Introduction

Nonsteroidal anti-inflammatory drugs (NSAIDs) are not only medicines for inflammation, but are also analgesic and antipyretic ones, and they are widely used for the treatment of a variety of human and veterinary disease conditions involving pain and inflammation management.[1,2] NSAIDs are some of the most widely used therapeutic drugs. Classic NSAIDs include (but not limited to) salicylates, arylalkanoic acids, aryl- and heteroaryl acetic acids, aryl- and heteroaryl propionic acids, *N*-aryl anthranilic acids (also known as fenamic acids, FAs), oxicams, *etc.*[3,4] These drugs exert their therapeutic effects by inhibiting prostaglandin (PG) synthesis through blocking the access of arachidonic acid to its binding site on the cyclooxygenase enzyme.[5,6] *N*-Aryl anthranilic acids are bio-isosteres of salicylic acid,[7] with mefenamic acid (MFA), flufenamic acid (FFA), clonixin (CLX), and flunixin (FLX) as representatives.[8] Among them, CLX and FLX are more closely related since they are both anilinonicotinic acids. Yet CLX is a human NSAID,[9] and FLX is a potent veterinary one widely used in horses and other livestock, in the form of meglumine salt, for the treatment of inflammatory diseases or colics.[10,11] Currently the application of FLX in human diseases is also explored.[12] FAs are conformationally flexible diarylamines. Polymorphism, *i.e.*, the formation of more than one crystal form of a given molecule, is widely observed in FAs and other compounds as multiple forms have been found for them.[13,14] For example, for mefenamic acid two polymorphs (**I** and **II**) have been

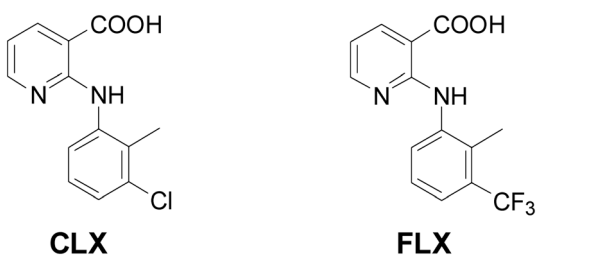

Scheme 1 Structures of CLX and FLX.

[a] *Key Laboratory for Green Chemical Process of Ministry of Education, Hubei Key Laboratory of Novel Reactor and Green Chemical Technology, Hubei Engineering Research Center for Advanced Fine Chemicals, School of Chemical Engineering and Pharmacy, Wuhan Institute of Technology, 206 1st Rd Optics Valley, East Lake New Technology Development District, Wuhan, Hubei 430205, China.*
E-mail: fyuwucn@gmail.com, Sihuilong@wit.edu.cn, longsihui@yahoo.com;
Tel: +027 87194980
[b] *Computational Center for Molecular Science, College of Chemistry, Nankai University, Tianjin, China*
[c] *Department of Chemistry, University of Kentucky, Lexington, Kentucky 40506, USA*
[d] *Department of Industrial and Physical Pharmacy, Purdue University, West Lafayette, Indiana 47907, USA*

† Electronic supplementary information (ESI) available: Two crystal structures of FLX in the form of crystallographic information file (CIF) were deposited in the Cambridge Crystallographic Data Centre (CCDC) with accession codes 1957482 and 1957486. For ESI and crystallographic data in CIF or other electronic format see DOI: 10.1039/c9ce01619h

‡ H. Liu and X. Yang contributed equally to this study.

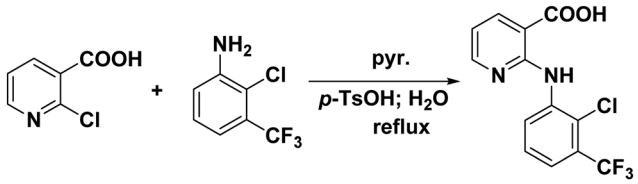

Scheme 2 Synthesis of FLX.

Table 1 Polymorph screening of FLX

Solvent	Growth conditions	Form
Ethyl acetate	Slow evaporation	**I**
Ethyl acetate	Slow cooling	**I**
Methanol	Slow evaporation	**I**
Methanol	Slow cooling	**I**
Ethanol	Slow evaporation	**I**
Ethanol	Slow cooling	**I**
Acetone	Slow evaporation	**I**
Acetone	Slow cooling	**I**
Acetonitrile	Slow evaporation	**I**
iso-Propanol	Slow evaporation	**I**
Water	Slow evaporation	**I**
Ether	Slow evaporation	**I**
Dichloromethane	Slow evaporation	**I**
Dimethylformamide	Slow evaporation	**I**
Acetic acid	Slow evaporation	**I**
Benzene	Slow evaporation	**I**
Dimethyl sulfoxide	Slow cooling	**I**

reported.[15] Nine polymorphs of FFA have been investigated,[16] and tolfenamic acid has been reported to have at least five forms.[17] In the past decade, our lab has investigated the pharmaceutical potential and polymorphism of FAs, particularly CLX and its derivatives.[8,18] A series of CLX and FA analogues have been synthesized and their polymorphic behavior has been studied experimentally and theoretically.[19] Among them, several highly polymorphic compounds stand out. For example, four forms have been discovered for 2-(phenylamino)nicotinic acid [2-PNA] and 2-[methyl(phenyl)-

Table 2 Crystallographic data of form I of CLX and FLX (both LT and RT)

	I (CLX)	FLX (LT)	FLX (RT)
Formula	$C_{13}H_{11}ClN_2O_2$	$C_{14}H_{11}F_3N_2O_2$	$C_{14}H_{11}F_3N_2O_2$
Formula weight	262.69	296.25	296.25
Crystal size (mm)	0.20 × 0.20 × 0.12	0.50 × 0.35 × 0.30	0.50 × 0.35 × 0.30
Crystal system	Monoclinic	Monoclinic	Monoclinic
Space group	$P2_1/c$	$P2_1/c$	$P2_1/c$
a/Å	7.479(1)	7.5380(1)	7.68546(13)
b/Å	14.162(2)	14.0607(2)	14.1282(2)
c/Å	11.582(2)	12.3766(1)	12.49862(17)
α/°	90.00	90.00	90.00
β/°	101.55(1)	103.3203(5)	102.1605(15)
γ/°	90.00	90.00	90.00
Z, Z'	4, 1	4, 1	4, 1
V/Å^3	1201.9(3)	1276.50(3)	1326.67(4)
D_{cal}/g cm^{-3}	1.452	1.542	1.483
T/K	90.0(2)	90.0(2)	293(2)
Abs coeff (mm^{-1})	0.312	0.134	1.120
F(000)	544	608	608
2θ range (deg)	2.30–27.50	2.23–25.98	4.4785–66.496
Limiting indices	$-9 \le h \le 9$	$-9 \le h \le 9$	$-7 \le h \le 8$
	$-18 \le k \le 18$	$-16 \le k \le 16$	$-16 \le k \le 16$
	$-15 \le l \le 15$	$-15 \le l \le 15$	$-14 \le l \le 14$
Completeness to 2θ	99.8%	98.2%	99.5%
Unique reflections	2264	2157	2037
$R_1[I > 2\sigma(I)]$	4.66	0.0391	0.0393
wR_2 (all data)	0.121	0.0971	0.1074

amino]nicotinic acid (2-MPNA), respectively.[20,21] Even for CLX, 30 years after the first report of its polymorphism, we have found that it tends to form solvates with DMF and DMF-like solvents.[8] In contrast, FLX was first synthesized in 1974[22] and ever since has been widely used in the control of pain and inflammation as a veterinary medicine and recently its effect on the uterine mobility of equine embryos has been investigated.[23] Yet, its polymorphism has never been studied.

In this work, we attempted to shed light on the solid state properties of FLX, a compound which closely resembles CLX structurally. As seen, the only difference between CLX and FLX is that Cl at the 3 position of CLX is replaced with CF_3 in FLX (Scheme 1), which is a strategy widely used in medicinal

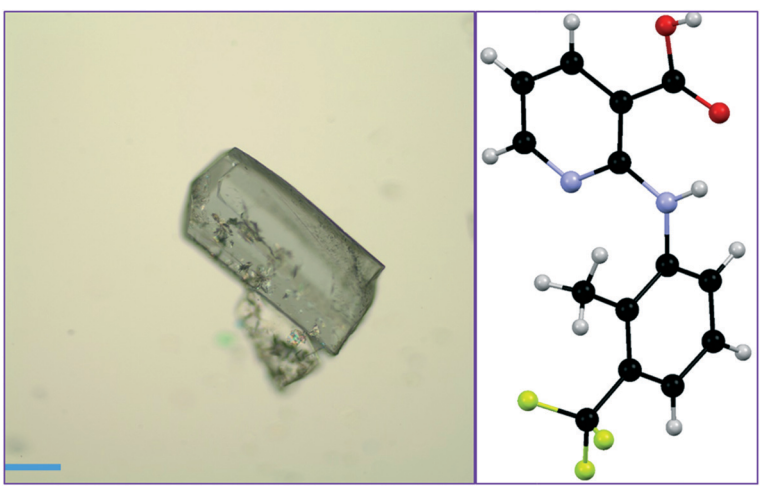

Fig. 1 Crystals and conformer of FLX. Scale bar 0.2 mm.

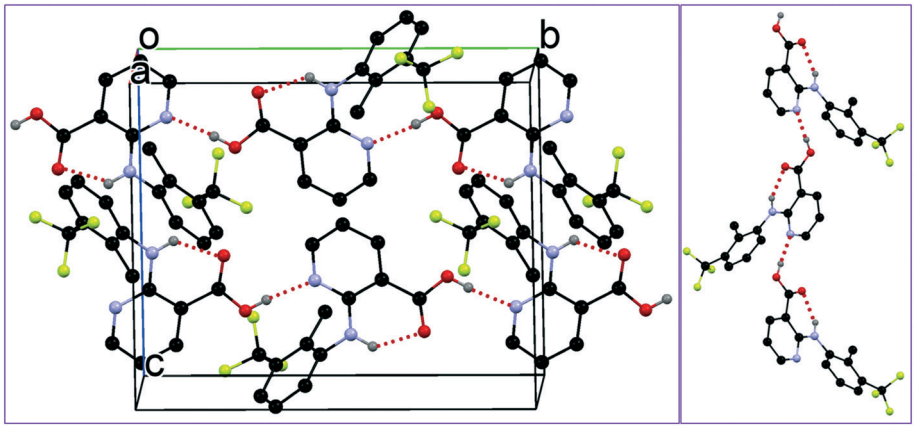

Fig. 2 Crystal packing of FLX (for clarity, hydrogens not involved in hydrogen bonding are omitted).

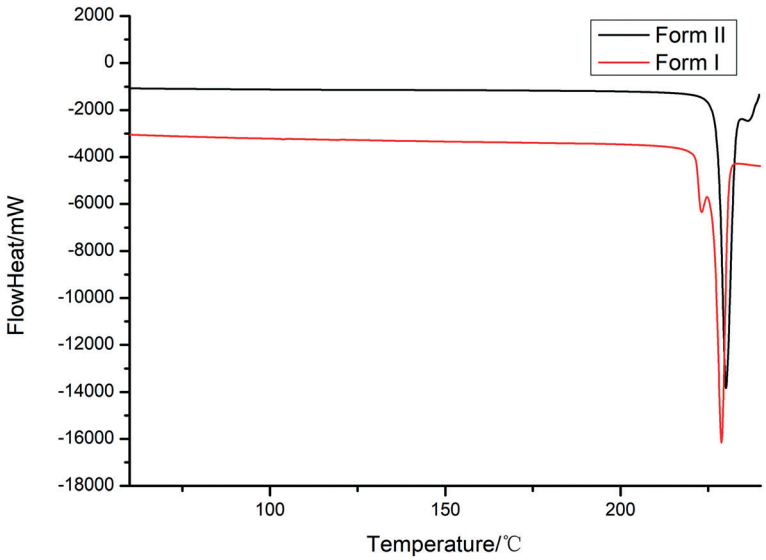

Fig. 3 DSC thermograms of FLX.

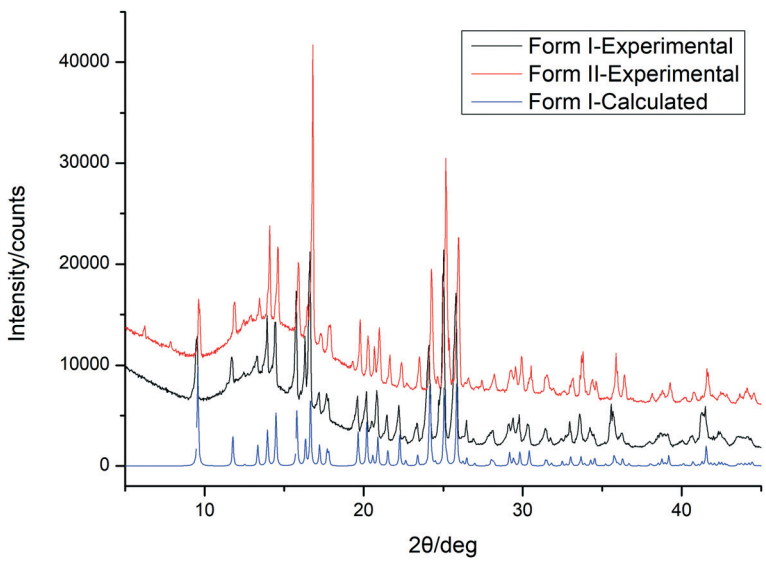

Fig. 4 PXRD patterns of the two forms of FLX.

Table 3 UNI intermolecular potentials in CLX crystals

Crystal form	Diagrammatic drawing	Types of interactions	Intermolecular potentials (kcal mol^{-1})	Number of contributions
I	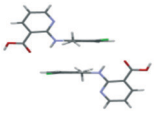	π–π stacking between two benzenes	−11.6	1
	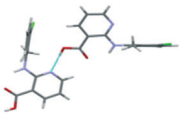	Hydrogen bond between carboxylic acid and pyridine	−10.0	2
	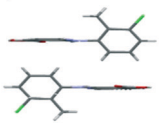	H–π stacking between H and pyridine	−8.2	1
	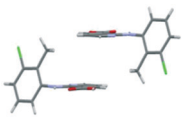	π–π stacking between two pyridines	−6.5	1
II (zwitterions)	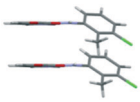	π–π stacking between two benzenes and two pyridines	−17.9	2
	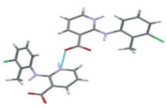	Hydrogen bond between carboxylate and pyridinium	−5.6	2
III	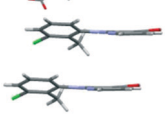	π–π stacking between two benzenes and two pyridines	−18.7	2
	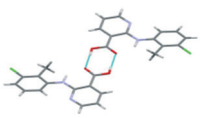	Hydrogen bond between two carboxylic acids	−9.5	1
IV		Antiparallel π–π stacking between benzene and pyridine	−18.8	2
	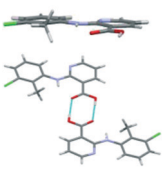	Hydrogen bond between two carboxylic acids	−9.5	1

chemistry.[24] Intuitively, we would expect FLX to be polymorphic, just like CLX. Yet, since CF_3 is not the same as Cl, difference in solid properties could be expected. In reality, only one form was obtained from crystallization in all the solvents used. Thus, we also tried to investigate the polymorphic behavior of FLX theoretically.

2. Experimental section

2.1. Materials

All chemicals were purchased from commercial sources: 2-methyl-3-trifluoromethyl-phenylamine was from Bide Pharmatech Ltd. (Shanghai, China), pyridine, 2-chloronicotinic acid and *p*-TsOH were from Aladdin Industrial Corporation, and solvents for crystal growth were from Sinopharm Chemical Reagent Co., Ltd. (Shanghai, China), and were used as received.

2.2. Synthesis

FLX was synthesized by reacting 2-chloronicotinic acid with 2-methyl-3-trifluoromethyl-phenylamine with *p*-TsOH as a catalyst under a nucleophilic aromatic substitution (SNAr) mechanism according to a literature procedure and purified by recrystallization from MeOH (Scheme 2).[20]

2-Chloronicotinic acid (2.0 g, 12.7 mmol) and 2-methyl-3-trifluoromethyl-phenylamine (1.8 g, 12.9 mmol) were suspended in pyridine (1.1 g, 13.7 mmol), and *p*-TsOH (0.6 g, 3.2 mmol) in 10 mL of water was added to the mixture. The resulting system was refluxed overnight and then it was

Table 4 UNI intermolecular potentials in FLX crystals

Crystal form	Diagrammatic drawing	Types of interactions	Intermolecular potentials (kcal mol^{-1})	Number of contributions
I	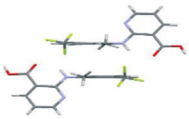	π–π stacking between two benzenes	−13	1
	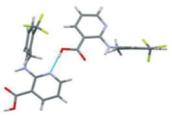	Hydrogen bond between carboxylic acid and pyridine	−10.3	2
	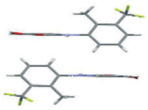	H–π stacking between H and pyridine	−7.2	1
	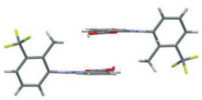	π–π stacking between two pyridines	−5.1	1

cooled to room temperature. The product precipitated and was recovered by filtration, and further purified by crystallization in MeOH (2.4 g, yield%: 73). The purity of the final product is over 99%.

^{1}H NMR (400 MHz, DMSO-d_6) δ ppm 10.30 (s, 1H), 8.34 (m, 1H), 8.27 (m, 1H), 8.11 (d, 1H), 7.19 (m, 2H), 6.87 (m, 1H), 2.33 (s, 3H); ^{13}C NMR (125 MHz, DMSO-d_6) δ ppm 169.7, 156.3, 153.1, 141.0, 140.3, 128.6, 127.7, 126.9, 126.2, 124.1, 120.6, 114.7, 108.4, 14.1; IR (KBr, cm^{-1}) 3239 (w), 2460 (w), 1677 (s), 1510 (s), 1242 (m), 1121 (s); EI-MS (MH^{+}) 297; mp 235 °C.

2.3. Crystallization

Since FLX and CLX are structurally similar, naturally we expected them to behave alike during crystallization. The same growth conditions used for CLX were applied to the crystal generation for FLX.[8] A detailed description of the procedure can be found in the ESI.† The same form was produced by slow evaporation in all the solvents used. Slow cooling was also used for crystal growth (see the ESI† for details). All crystallization experiments were conducted in an unmodified atmosphere. The identity of the crystals was confirmed by either single-crystal X-ray or powder X-ray diffraction. The crystallization results are listed in Table 1.

2.4. Characterization

The crystal structure of FLX was determined by single-crystal X-ray diffraction (SCXRD). Powder X-ray diffraction (PXRD) was applied for the bulk sample. The thermal behavior of FLX was investigated by differential scanning calorimetry (DSC). IR and Raman spectra were measured for the FLX samples. The experimental details for each characterization are described in the ESI.†

2.5. Computational details

Gavezzotti's UNI intermolecular potentials of all the crystals were investigated first.[25,26] All the CLX dimers were extracted from the experimental crystal structures. FLX dimers were simulated by substituting the Cl in their corresponding CLX forms with CF_3 in order to compare and explain the difference between CLX and FLX. All dimers discussed here were optimized at the B3LYP/6-311G** level with dispersion corrections (GD3BJ)[27] using Gaussian16.[28] Single point energy calculations based on the optimized structures were performed with a larger basis set (6-311+G**). For both optimization and single point calculations, solvation was implicitly accounted for using the SMD[29] continuum solvation model. Three typical solvents, water (H_2O), benzene, and dichloromethane (DCM), were selected based on their polarity difference. All calculations were performed at 1 atm and 298.15 K. Stabilization energy (ΔE) was defined as $\Delta E = E(\text{dimer}) - 2 \times E(\text{monomer})$, in which E(monomer) refers to the energy of the optimized single molecule in the corresponding solvent, and E(dimer) refers to the energy of the optimized dimer. The sum of the stabilization energies of the assumed dimers was used to estimate and compare the thermodynamic stabilities of the possible corresponding crystal forms between CLX and FLX. The relaxed potential energy surface scan for the dihedral angle was conducted at B3LYP/6-311+G** with a step of 10 degrees. Hirshfeld surface analysis[30,31] was carried out and its fingerprint plot revealed intermolecular contacts within the crystal structure, providing insight into the intermolecular interactions. The relative contributions of various interactions to the Hirshfeld surface were calculated using CrystalExplorer.[32]

3. Results and discussion

3.1. Crystal structures

In contrast to the four solvent-free polymorphic forms and one solvate found for CLX, only one crystal form

Table 5 Stabilization energies for CLX dimers in different solvents

Original structures extracted from the crystal form	Diagrammatic drawing	Types of dimers	Solvent		
			ΔE (kcal mol^{-1}) in H_2O	ΔE (kcal mol^{-1}) in benzene	ΔE (kcal mol^{-1}) in DCM
I	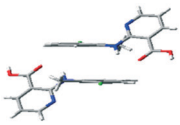	π–π stacking between two benzenes	−14.34	−8.85	−9.37
	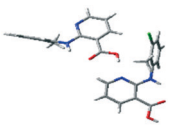	Hydrogen bond between carboxylic acid and pyridine	−12.79	−13.33	−12.50
	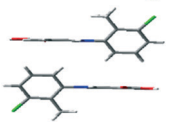	H–π stacking between H and pyridine	−19.53	−8.58	−13.40
	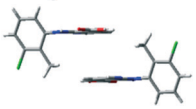	π–π stacking between two pyridines	−13.77	−6.26	−7.35
II (zwitterions)	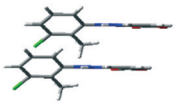	π–π stacking between two benzenes and two pyridines	−28.21	NA	−4.70
	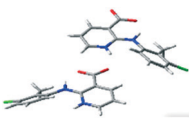	Hydrogen bond between carboxylate and pyridinium	−19.37	0.60	−10.49
III	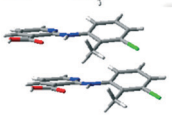	π–π stacking between two benzenes and two pyridines	−20.47	−14.05	−14.49
	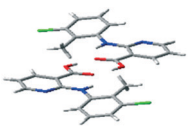	Hydrogen bond between carboxylic acid and pyridine	−11.86	−16.67	−13.90
IV	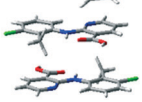	Antiparallel π–π stacking between benzene and pyridine	−22.05	−17.22	−16.45
	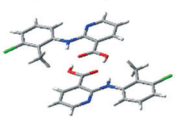	Hydrogen bond between two carboxylic acids	−11.65	−16.67	−13.79

was obtained for FLX through crystallization in all the solvents used. No solvate was harvested from DMF. The crystal is monoclinic, space group $P2_1/c$ (Z = 4). The crystallographic data of form **I** (both LT and RT) and CLX-**I** are listed in Table 2; complete CIF files are provided in the ESI.† There is one formula unit in the asymmetric unit. These crystallographically independent molecules are conformationally similar to those in CLX-**I**-LT as suggested by the dihedral angle between the two aromatic rings in the molecules (68.22 (5)° for CLX-**I**-LT, 69.97(4)° for FLX (LT) and 71.14 (5)° for FLX (RT), respectively) (Fig. 1).

The crystal structure of FLX is isostructural to that of CLX form **I** as can be seen from the crystallographic data. The molecule in the asymmetric unit is highly twisted as suggested by the dihedral angle of 69.97 (4)° between the pyridine ring and the benzene ring, similar to that of 68.22 (5)° in CLX-**I**. Due to the nonplanarity of the molecule, the crystals are colorless and the energetically more favorable hydrogen bond between the carboxylic acid and pyridine N is observed (C(6) in graph-set notation).[32,33] This is in agreement with the general rule established in our recent study regarding the formation of either the acid–acid homosynthon or the acid–pyridine heterosynthon in 2-PNA

Table 6 Stabilization energies for FLX dimers in different solvents

Assumed dimers corresponding to the CLX crystal form	Diagrammatic drawing	Types of dimers	Solvent		
			ΔE (kcal mol^{-1}) in H_2O	ΔE (kcal mol^{-1}) in benzene	ΔE (kcal mol^{-1}) in DCM
I	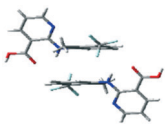	π–π stacking between two benzenes	−14.12	−8.43	−9.01
	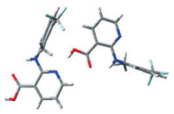	Hydrogen bond between carboxylic acid and pyridine	−12.10	−12.78	−12.09
	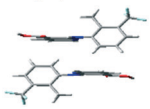	H–π stacking between H and pyridine	−18.72	−5.52	−6.22
	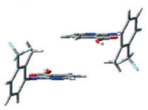	π–π stacking between two pyridines	−13.60	−5.98	−6.92
II (zwitterions)	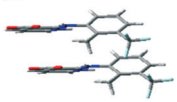	π–π stacking between two benzenes and two pyridines	−23.38	−1.68	−9.56
	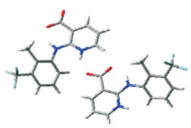	Hydrogen bond between carboxylate and pyridinium	−18.00	0.00	−10.91
III	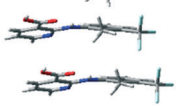	π–π stacking between two benzenes and two pyridines	−18.98	−13.65	−14.55
	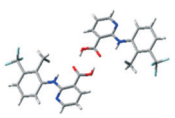	Hydrogen bond between two carboxylic acids	−11.39	−16.55	−13.80
IV		Antiparallel π–π stacking between benzene and pyridine	−20.76	−15.83	−15.08
	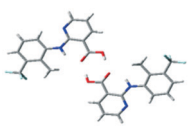	Hydrogen bond between two carboxylic acids	−11.55	−16.57	−13.81

analogues, *i.e.*, if the dihedral angle between the pyridine ring and the benzene ring is over 30°, the acid–pyridine heterosynthon will be formed, otherwise the acid–acid homosynthon will be formed.[34] The hydrogen bond parameters are 1.846 Å for the bond length and 173.73° for the bond angle. Other than the intermolecular hydrogen bond, there is also an intramolecular hydrogen bond in each molecule between the NH that bridges the two aromatic rings and the carbonyl O of the carboxylic acid (S6), with a bond length of 1.961 Å and a bond angle of 134.79° (Fig. 2).

3.2. Thermal properties

We resorted to DSC to investigate the thermal properties of FLX, and the DSC thermogram is shown in Fig. 3. Upon heating, the crystals grown from different solvents showed two thermal events, the minor one with an onset temperature of 220 °C which seemed to be a phase transition which led to a new form and the major one next to it with an onset temperature of 227 °C, which was the melting of the new form. To confirm the formation of the new polymorph, the sample was cooled down to room temperature when it was heated right after the phase transition temperature, and when the new form was heated again, only one thermal event was observed (Fig. 3).

Fig. 4 shows the powder X-ray diffraction patterns of the crystals grown from solvents and obtained after thermal treatment of the original crystals, along with the PXRD pattern of form **I** calculated from the single-crystal structure determined at 293 K.

3.3. Computational results

The only difference between CLX and FLX was that Cl at the 3 position of CLX was replaced with CF_3 in FLX. CLX is known to exist in four solvent-free forms and at least one solvate crystal form, namely forms **I**, **II**, **III**, **IV**, and **S**. However, only one crystal form has been obtained from solution for FLX in this study. Theoretical calculations were made to compare and explain the polymorphism difference of CLX and FLX.

First, we tried to find out the dimers with strong interactions in all the known crystal forms according to Gavezzotti's UNI intermolecular potentials. The results are listed in Tables 3 and 4. From the results we could conclude that the hydrogen bond dimers as well as π–π stacking dimers dominated the crystal structures.

All dimers with their relative energies are listed in Tables 5 and 6. The total energies of the assumed crystals were then calculated based on the corresponding dimers and their contribution to different crystals. The summed up interaction energies were then compared as shown in Table 7 to discuss the thermodynamic stability of the assumed crystals.

The single molecule in CLX form **II** was a zwitterion; however, zwitterions are not stable in non-polar solvents, so form **II** was excluded from the non-polar solvent benzene. In addition, the FLX dimer with an acid–pyridine hydrogen bond found in FLX form **I** would rotate along the hydrogen bond axis, so the restricted optimization was conducted for this dimer with the dihedral angle of the hydrogen bond plane fixed.

Our calculations reasonably explained why CLX and FLX mainly formed form **I** in water from the perspective of thermodynamics. According to the data, we could find that form **I** would be 20 kcal mol^{-1} thermodynamically lower than forms **III** and **IV**.

Our calculations also explained why CLX and FLX could generate form **I** in dichloromethane. For CLX, a thermodynamic difference of −55.14 kcal mol^{-1} could be obtained for the formation of form **I**, which was more stable than those for the formation of forms **III** and **IV**, which were −42.89 kcal mol^{-1} and −46.69 kcal mol^{-1}, respectively. As for FLX, the thermodynamic difference value of form **I** was −46.33 kcal mol^{-1}, which was also more stable than those for the formation of forms **III** and **IV**, which were −42.90 kcal mol^{-1} and −43.96 kcal mol^{-1}, respectively. Therefore, the formation of form **I** could also be explained with its thermodynamic stability.

Our calculations reasonably explained the formation of form **IV** in benzene for CLX. The thermodynamic difference value was −51.11 kcal mol^{-1} for form **IV** in benzene, while the values of forms **I** and **III** were −50.14 kcal mol^{-1} and −44.76 kcal mol^{-1}, respectively. Intriguingly, a similar trend was found for FLX calculations, which were not consistent with the experimental results. The limitation of calculations may be a possible explanation for this. A restricted optimization was adopted to avoid the rotation of the hydrogen bond axis when we optimized the acid–pyridine hydrogen bond dimers for FLX, which would give a higher energy for the unstable structure, while FLX molecules can form acid–pyridine hydrogen bond chains experimentally with the adjacent molecules hindering the rotation. Additionally, the growth of long chains will decrease the polarity of the molecules and thus further decrease the repulsion from the nonpolar solvents. Therefore, the stability of form **I** was underestimated by the limitation of calculations. The thermodynamic difference for form **I** of FLX was calculated to be −45.5 kcal mol^{-1}, which was insufficient to compete with the thermodynamic difference of −48.22 kcal mol^{-1} for form **IV**. Moreover, there are still many other factors affecting the crystallization including kinetic reasons which were not investigated here.

The relaxed potential energy surface (PES) evaluation was carried out *via* the flexible scanning of the dihedral angle C2–N7–C8–C9 (τ) of FLX based on its optimized structure. It can be found that there are two stable conformations (Fig. 5):

Table 7 The sum of the stabilization energies (ΔE) of assumed dimers of CLX and FLX in different solvents

Corresponding crystal form	Solvent	ΔE of CLX (kcal mol^{-1})	ΔE of FLX (kcal mol^{-1})
I	Water	−73.22	−70.64
	Benzene	−50.35	−45.50
	Dichloromethane	−55.14	−46.33
II	Water	−95.17	−82.75
	Benzene	NA	−3.36
	Dichloromethane	−30.38	−40.93
III	Water	−52.80	−49.36
	Benzene	−44.76	−43.84
	Dichloromethane	−42.89	−42.90
IV	Water	−55.74	−53.07
	Benzene	−51.11	−48.22
	Dichloromethane	−46.69	−43.96

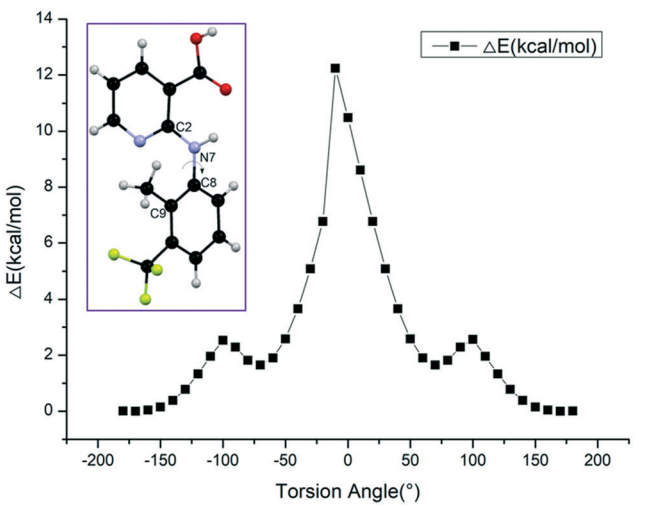

Fig. 5 Relaxed potential energy surface (PES) scan along C2–N7–C8–C9.

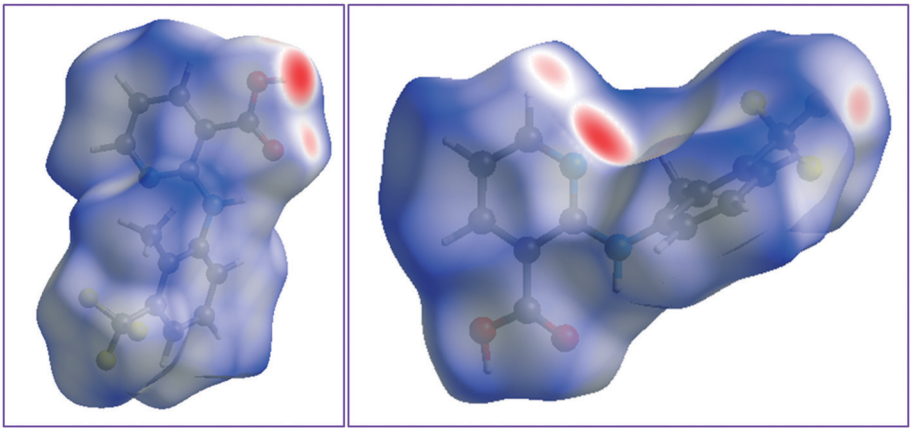

Fig. 6 Hirshfeld surface with different orientations.

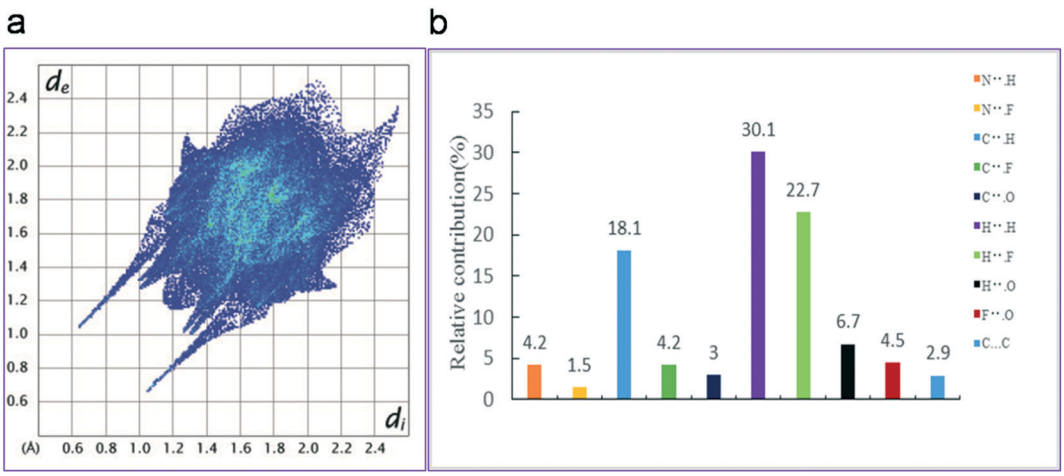

Fig. 7 a. 2D fingerprint plots for FLX; b. relative contributions to the Hirshfeld surface by the various intermolecular contacts in the crystal.

the nearly planar one with τ near 170° and the twisted one with τ near 70° (τ = 68.3° in the crystal). The energy difference is less than 2 kcal mol^{-1}, and the rotation energy barrier between them is only about 2.5 kcal mol^{-1}. This suggests that the two conformations could be transformed freely with a dynamic equilibrium. Further optimizations of the two conformations were conducted, where the energy of the twisted conformation (τ = 70.7°) is slightly higher than that of the nearly planar one (τ = 172.4°) by only 1.36 kcal mol^{-1} including zero point energy (ZPE) correction, or 2.11 kcal mol^{-1} in Gibbs free energy.

In Fig. 6, it is evident that there are dominant interactions represented by the bright red spots, which are caused by the hydrogen bond interaction between the N atom of pyridine and the H atom of the carboxylic acid. This dominant interaction is also represented by two spikes in the left-bottom region of the fingerprint plot (Fig. 7). Other close contacts were also counted with their contributions to the Hirshfeld surface area in Fig. 7. H–π interactions can be seen with C···H contacts with 18.1% of the Hirshfeld surface. H···F contacts can also be found with a proportion of 22.7%. π···π stacking interactions were represented by C···C contacts with a proportion of 2.9%. Hirshfeld surface analysis provided us a better understanding of the interactions of molecules in the crystal.

4. Conclusions

FLX was synthesized through an SNAr reaction and two crystal forms were obtained, one (**I**) through crystallization in solvents and the other (**II**) through thermal phase transition. Form **I** was fully characterized by SCXRD, PXRD, FT-IR and Raman spectroscopy. The crystal structure of form **I** is sustained on the acid–pyridine heterosynthon, same as that observed in form **I** of CLX. Form **I** transforms into form **II** upon thermal treatment. Theoretical calculations were performed to explain the lack of polymorphism in different solvents. Potential energy surface scan discloses two energetically close conformations, one with a torsion angle of 170° and the other 70°, which corresponds to the experimental conformation in the crystal. Hirshfeld analysis further delineates the contribution of individual interactions

to the overall stability of each form. Considering the close resemblance between FLX and CLX, the "lack" of polymorphism for FLX deserves further investigation.

Conflicts of interest

There are no conflicts of interest to declare.

Acknowledgements

SL thanks the Natural Science Foundation of Hubei Province for financial support (2014CFB787). HL acknowledges the sponsorship from the Innovation Fund of the Graduate School (CX2018003). TL is grateful to NSF for supporting this work (DMR1006364). SP is grateful to the NSF MRI program (CHE0319176 and CHE1625732).

References

1 S. Bajaj, S. S. Sambi and A. K. Madan, *Bioorg. Med. Chem.*, 2004, **12**, 3695.
2 P. Patrignani and C. Patrono, *Biochim. Biophys. Acta, Gen. Subj.*, 2015, **1851**, 422–432.
3 J. S. Kaltenbronn, R. A. Scherrer, F. W. Short, E. M. Jones, H. R. Beatty, M. M. Saka, C. V. Winder, J. Wax and W. R. Williamson, *Arzneim. Forsch.*, 1983, **33**, 621–627.
4 J. R. O'Brien, D. M. Oxon and F. C. Path, *Lancet*, 1968, **291**, 779–783.
5 G. A. Green, *Clin. Cornerstone*, 2001, **3**, 50–59.
6 A. K. Dwivedi, V. Gurjar, S. Kumar and N. Singh, *Drug Discovery Today*, 2015, **20**, 863–873.
7 R. Hu, Y. Zhoujin, M. Liu, M. Zhang, S. Parkin, P. Zhou, J. Wang, F. Yu and S. Long, *RSC Adv.*, 2018, **8**, 15459–15470.
8 S. Long, T. Mao, P. Chen, M. Liu, S. Parkin, M. Zhang, T. Li, P. Zhou and F. Yu, *ChemistrySelect*, 2017, **2**, 4942–4950.
9 J. M. Lee, K. M. Park, S. J. Lim, M. K. Lee and C. K. Kim, *J. Pharm. Pharmacol.*, 2002, **54**, 43–49.
10 J. E. Tomlinson, B. O. Wilder, K. M. Young and A. T. Blikslager, *Am. J. Vet. Res.*, 2004, **65**, 761–769.
11 S. Zamir, A. Rozov and E. Gootwine, *Vet. Rec.*, 2009, **165**, 265–266.
12 I. Reinholds, I. Pugajeva, D. Zacs, E. Lundanes, J. Rusko, I. Perkons and V. Bartkevics, *Environ. Monit. Assess.*, 2017, **189**, 568.
13 A. Kons, A. Berzin, A. Actiņs, T. Rekis, S. Smaalen and A. Mishnev, *Cryst. Growth Des.*, 2019, **19**, 4765–4773.
14 B. Hachuła, M. Zubko, P. Zajdel, M. Książek, J. Kusz, O. Starczewska, J. Janeka and W. Pisarski, *CrystEngComm*, 2018, **20**, 1739–1745.
15 F. Kato, M. Otsuka and Y. Matsuda, *Int. J. Pharm.*, 2006, **321**, 18–26.
16 V. Lópezmejías, J. W. Kampf and A. J. Matzger, *J. Am. Chem. Soc.*, 2012, **134**, 9872–9875.
17 W. Tang, H. Mo, M. Zhang, S. Parkin, J. Gong, J. Wang and T. Li, *J. Phys. Chem. B*, 2017, **121**, 10118–10124.
18 M. Liu, G. Shen, Z. Yuan, S. Parkin, F. Yu, M. Zhang, S. Long and T. Li, *Cryst. Growth Des.*, 2018, **18**, 7006–7014.
19 Y. Liu, M. Zhang, D. Xu, S. Parkin, T. Li, C. Li, Z. Yang, F. Yu and S. Long, *Cryst. Growth Des.*, 2019, **19**, 3694–3703.
20 S. Long, S. Parkin, M. A. Siegler, A. Cammers and T. Li, *Cryst. Growth Des.*, 2008, **8**, 4006–4013.
21 S. Long, S. Parkin, M. Siegler, C. P. Brock, A. Cammers and T. Li, *Cryst. Growth Des.*, 2008, **8**, 3137–3140.
22 M. H. Sherlock, *US Pat.*, 3839344, 1974.
23 C. T. C. Okada, V. P. Andrade, C. P. F. Dell'Aqua, M. Nichi, C. B. Fernandes, F. O. Papa and M. A. Alvarenga, *Theriogenology*, 2019, **123**, 132–138.
24 Y. Sasaki, M. Hirabuki, A. Ambo, H. Ouch and Y. Yamamoto, *Bioorg. Med. Chem. Lett.*, 2001, **11**, 327–329.
25 A. Gavezzotti, *Acc. Chem. Res.*, 1994, **27**, 309–314.
26 A. Gavezzotti and G. Filippini, *J. Phys. Chem.*, 1994, **98**(18), 4831–4837.
27 S. Grimme, S. Ehrlich and L. Goerigk, *J. Comput. Chem.*, 2011, **32**, 1456–1465.
28 M. J. Frisch, G. W. Trucks, H. B. Schlegel, G. E. Scuseria, M. A. Robb, J. R. Cheeseman, G. Scalmani, V. Barone, G. A. Petersson, H. Nakatsuji, X. Li, M. Caricato, A. V. Marenich, J. Bloino, B. G. Janesko, R. Gomperts, B. Mennucci, H. P. Hratchian, J. V. Ortiz, A. F. Izmaylov, J. L. Sonnenberg, D. Williams-Young, F. Ding, F. Lipparini, F. Egidi, J. Goings, B. Peng, A. Petrone, T. Henderson, D. Ranasinghe, V. G. Zakrzewski, J. Gao, N. Rega, G. Zheng, W. Liang, M. Hada, M. Ehara, K. Toyota, R. Fukuda, J. Hasegawa, M. Ishida, T. Nakajima, Y. Honda, O. Kitao, H. Nakai, T. Vreven, K. Throssell, J. A. Montgomery Jr, J. E. Peralta, F. Ogliaro, M. J. Bearpark, J. J. Heyd, E. N. Brothers, K. N. Kudin, V. N. Staroverov, T. A. Keith, R. Kobayashi, J. Normand, K. Raghavachari, A. P. Rendell, J. C. Burant, S. S. Iyengar, J. Tomasi, M. Cossi, J. M. Millam, M. Klene, C. Adamo, R. Cammi, J. W. Ochterski, R. L. Martin, K. Morokuma, O. Farkas, J. B. Foresman and D. J. Fox, *Gaussian 16, Revision A.03*, Gaussian, Inc., Wallingford, CT, 2016.
29 A. V. Marenich, C. J. Cramer and D. G. Truhlar, *J. Phys. Chem.*, 2009, **113**, 6378–6396.
30 F. L. Hirshfeld, *Theor. Chim. Acta*, 1977, **44**, 129–138.
31 M. A. Spackman and D. Jayatilaka, *CrystEngComm*, 2009, **11**, 19–32.
32 S. K. Wolff, D. J. Grimwood, J. J. McKinnon, M. J. Turner, D. Jayatilaka and M. A. Spackman, *Crystal Explorer 2.0*, University of Western Australia, 2012.
33 M. C. Etter, *Acc. Chem. Res.*, 1990, **23**, 120–126.
34 J. Bernstein and R. E. Davis, *Angew. Chem., Int. Ed. Engl.*, 1995, **34**, 1555–1573.